Journal of Pathology
*J Pathol* January 2022; **256:** 93–107
Published online 18 November 2021 in Wiley Online Library (wileyonlinelibrary.com) DOI: 10.1002/path.5812

ORIGINAL PAPER

# Homozygous *WASHC4* variant in two sisters causes a syndromic phenotype defined by dysmorphisms, intellectual disability, profound developmental disorder, and skeletal muscle involvement

Andrea Gangfuß[1*], Artur Czech[2], Andreas Hentschel[2], Ute Münchberg[2], Rita Horvath[3], Ana Töpf[4], Emily O'Heir[5], Hanns Lochmüller[6,7,8], Florian Stehling[9], Cordula Kiewert[10], Albert Sickmann[2], Alma Kuechler[11,12], Frank J. Kaiser[11,12], Heike Kölbel[1], Jon Christiansen[1], Ulrike Schara-Schmidt[1] and Andreas Roos[1,8]

[1] *Department of Pediatric Neurology, Centre for Neuromuscular Disorders, Centre for Translational Neuro- and Behavioral Sciences, University Duisburg-Essen, Essen, Germany*
[2] *Leibniz-Institut für Analytische Wissenschaften – ISAS – e.V., Dortmund, Germany*
[3] *Department of Clinical Neurosciences, John Van Geest Centre for Brain Repair, School of Clinical Medicine, University of Cambridge, Cambridge, UK*
[4] *The John Walton Muscular Dystrophy Research Centre, Translational and Clinical Research Institute, Newcastle University and Newcastle Hospitals NHS Foundation Trust, Newcastle upon Tyne, UK*
[5] *Center for Mendelian Genomics, Program in Medical and Population Genetics, Broad Institute of MIT and Harvard, Cambridge, MA, USA*
[6] *Department of Neuropediatrics and Muscle Disorders, Medical Center – University of Freiburg, Faculty of Medicine, Freiburg, Germany*
[7] *Centro Nacional de Análisis Genómico (CNAG-CRG), Center for Genomic Regulation, Barcelona Institute of Science and Technology (BIST), Barcelona, Spain*
[8] *Children's Hospital of Eastern Ontario Research Institute; Division of Neurology, Department of Medicine, The Ottawa Hospital; and Brain and Mind Research Institute, University of Ottawa, Ottawa, Canada*
[9] *Children's Hospital, Department of Pneumology, University Hospital Essen, Essen, Germany*
[10] *Children's Hospital, Department of Endocrinology, University Hospital Essen, Essen, Germany*
[11] *Institute of Human Genetics, University Hospital Essen, University Duisburg-Essen, Essen, Germany*
[12] *Essener Zentrum für seltene Erkrankungen (EZSE), University Hospital Essen, University Duisburg-Essen, Essen, Germany*

**Correspondence to: A Gangfuß, Department of Pediatric Neurology, Centre for Neuromuscular Disorders, Centre for Translational Neuro- and Behavioral Sciences, University Duisburg-Essen, Faculty of Medicine, University Hospital Essen, Hufelandstraße 55, 45122 Essen, Germany. E-mail: andrea.gangfuss@uk-essen.de*

## Abstract

**Recessive variants in *WASHC4* are linked to intellectual disability complicated by poor language skills, short stature, and dysmorphic features. The protein encoded by *WASHC4* is part of the Wiskott–Aldrich syndrome protein and SCAR homolog family, co-localizes with actin in cells, and promotes Arp2/3-dependent actin polymerization *in vitro*. Functional studies in a zebrafish model suggested that *WASHC4* knockdown may also affect skeletal muscles by perturbing protein clearance. However, skeletal muscle involvement has not been reported so far in patients, and precise biochemical studies allowing a deeper understanding of the molecular etiology of the disease are still lacking. Here, we report two siblings with a homozygous *WASHC4* variant expanding the clinical spectrum of the disease and provide a phenotypical comparison with cases reported in the literature. Proteomic profiling of fibroblasts of the WASHC4-deficient patient revealed dysregulation of proteins relevant for the maintenance of the neuromuscular axis. Immunostaining on a muscle biopsy derived from the same patient confirmed dysregulation of proteins relevant for proper muscle function, thus highlighting an affliction of muscle cells upon loss of functional WASHC4. The results of histological and coherent anti-Stokes Raman scattering microscopic studies support the concept of a functional role of the WASHC4 protein in humans by altering protein processing and clearance. The proteomic analysis confirmed key molecular players *in vitro* and highlighted, for the first time, the involvement of skeletal muscle in patients.**



**Keywords:** KIAA1033; WASHC4; intellectual disability; dysmorphisms; fibroblast proteomics; muscle autophagy; valosin-containing protein; coherent anti-Stokes Raman scattering microscopy

Received 12 March 2021; Revised 1 September 2021; Accepted 29 September 2021

*No conflicts of interest were declared.*

## Introduction

Intellectual disability has an estimated prevalence of 1.5–2%, and whole exome sequencing studies have identified a multitude of novel causative genes [1]. Recessive variants in *WASHC4* were linked to intellectual disability complicated by poor language skills, short stature, and dysmorphic features. Strumpellin (*WASHC5*) mutations are associated with

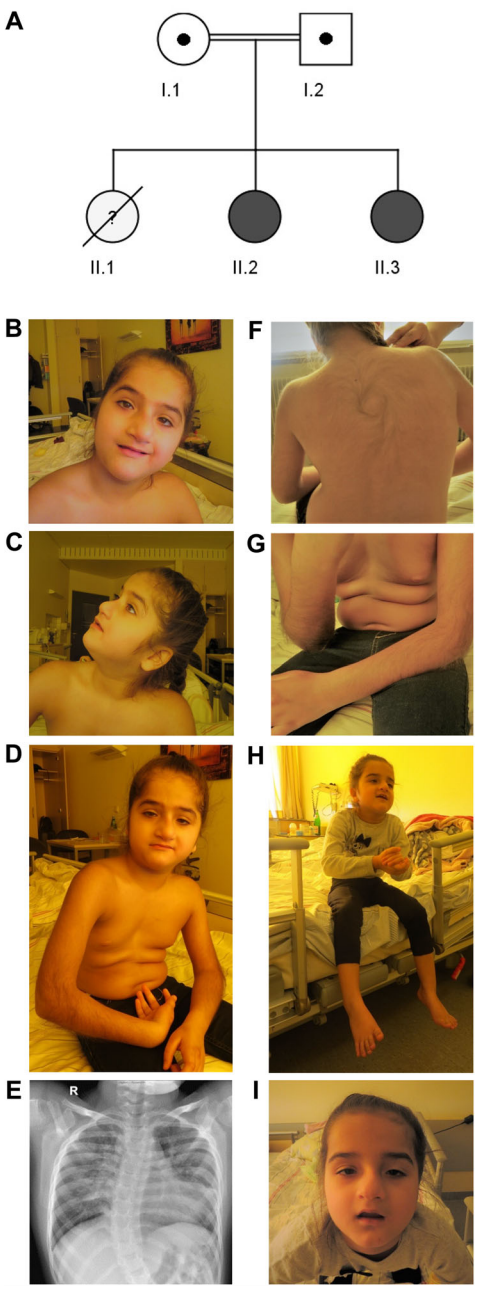


**Figure 1.** Clinical findings. (A) Family pedigree: I.1 and I.2: healthy, consanguineous parents (cousins I°) of Middle Eastern descent (United Arab Emirates). II.1: first female child, born at 29 weeks of gestation, died 4 days after birth due to unknown cause. II.2: sibling 1, *WASHC4* patient 11. II.3: sibling 2, *WASHC4* patient 12. (B–I) Clinical phenotype. Sibling 1: (B) Facial dysmorphic features: enlarged and coarsened nasal tip with deviation to the left side, small upper lip vermilion, small eyes with moderate ptosis and mild strabismus, high arched eyebrows, and discreet synophrys. (C) Low-set ears with enlarged ear lobes, and prominent forehead with low-set hairline. (D) Generalized muscle hypotonia. (E) X-ray of thorax in supine position showing bipulmonary infiltrations and right convex scoliosis. (F, G) General hirsutism, predominantly on the back and forearms. Sibling 2: (H, I) Stereotype movements of the hands and facial dysmorphic features: enlarged and coarsened nasal tip with deviation to the right side; small eyes with moderate ptosis and low-set ears. Informed consent to publish photographs was obtained for both patients.

neurological disease and causative for hereditary spastic paraplegia [2] and cranio-cerebello-cardiac dysplasia (Ritscher–Schinzel syndrome) [3].

The Wiskott–Aldrich syndrome protein (WASP) family is known for its participation in cytoskeleton reorganization [4,5]. In 2007, the human subtelomeric MGC52000 genes were renamed as Wiskott–Aldrich syndrome protein and SCAR homolog (WASH). Human WASH proteins are part of the WASP family, co-localize with actin in cells, and promote Arp2/3-dependent actin polymerization *in vitro* [6]. The WASH multiprotein complex consists of seven subunits: notably Strumpellin and WAS protein family homolog (WASH)-interacting protein (SWIP), which is encoded by the *WASHC4* gene, FAM21, and Arp2/3. The Arp2/3-dependent actin polymerization from G-actin to F-actin is an important step in regulation of the cytoskeleton, enabling multiple endosomal transport processes [7,8]. Linardopoulou *et al* have shown in *Drosophila* that the single WASH ortholog is essential for viability [6], strengthening the concept that *WASHC4* plays a crucial role in muscle cell integrity and function.

WASHC4/SWIP is an important interactor of valosin-containing protein (VCP). VCP is a key regulator of cellular proteostasis by regulating protein turnover and quality control. Mutations in VCP lead to severe myodegenerative and neurodegenerative diseases such as inclusion body myopathy with Paget disease of the bone and frontotemporal dementia (IBMPFD). By using the zebrafish (*Danio rerio*) vertebrate model, Kustermann *et al* were able to show that targeted inactivation of either VCP or WASHC4 leads to progressive impairment of muscle function, structure, and cytoarchitecture. Moreover, they proved that loss of VCP resulted in compromised protein degradation via the proteasome and the macroautophagy/autophagy machinery. In contrast, WASHC4 deficiency did not affect the function of the ubiquitin-proteasome system (UPS) but caused ER stress and interfered with autophagy function [9].

A link between autosomal recessive intellectual disability (ARID) and mutations in the *WASHC4* gene was first recognized in 2011 by Ropers and co-workers. They described a large consanguineous family with seven affected individuals (five females, two males), all suffering from moderate to severe intellectual disability (ID) (IQ 35–50) due to a homozygous missense variant in exon 29 of the *WASHC4* gene (c.3056C>G, p.Pro1019Arg). Other common features were poor language skills and short stature but no dysmorphic features [10] (supplementary material, Table S1).

Based on this publication, the *WASHC4* gene (MIM *615748) on chromosome 12q23 was listed in OMIM as the gene responsible for non-syndromic autosomal recessive mental retardation (MRT43, MIM #615817). Very recently, Assoum *et al* reported three additional patients from two unrelated families with syndromic ID. Two of them were sisters (8 and 6 years old), both presenting with learning disabilities, macrocephaly, dysmorphic features, skeletal anomalies, and subependymal heterotopic nodules due to a compound heterozygous mutation in the *WASHC4* gene [p.(Gln442*) and

p.(Asp1048Gly)]. The third patient was a 34-year-old female with mild ID, behavioral anomalies, short stature, microcephaly, dysmorphic facial features, and hyperpilosity resulting from a compound heterozygous mutation of the *WASHC4* gene [p.(Lys1079Arg) and p.(His503Arg)] [11] (supplementary material, Table S1).

The *WASHC4* variant [c.3041A>G; p.(Tyr1014Cys)] present in the sisters described in this study was assessed as a variant of uncertain significance (VUS) by Reuter *et al* in 2017 and was mentioned in the supplemental material belonging to the article [12]. As early as 1999, Kikuno *et al* described the expression of KIAA1033 (WASHC4) in the brain, which explains neurodevelopmental delay and ID [13]. Recently, Courtland *et al* reported endo-lysosomal dysfunction and cognitive-movement impairments in mice and humans due to genetic disruption of *WASHC4* [14].

In this study, we precisely describe the clinical phenotype of the two sisters and provide additional information (histological and proteomic data) derived from skin and muscle biopsy of the elder sibling to confirm the pathogenicity of the reported variant and establish the function of WASHC4 as relevant for muscle homeostasis.

## Materials and methods

### Ethics approval and consent to participate

Parental informed consent including permission to publish data and photographs was obtained for both patients, and the ethics committee of University Medicine Essen granted ethical approval (19-9011-BO). All procedures involving human subjects were in accordance with the Declaration of Helsinki 1975, as revised in 1983.

### Exome sequencing

Whole exome sequencing (WES) was performed by the Genomics Platform at the Broad Institute of MIT and Harvard (Cambridge, MA, USA). Libraries were created with an Illumina (San Diego, CA, USA) exome capture (38 Mb target) and sequenced with a mean target coverage of >80x. Exome sequencing data were processed and analyzed on the RD-Connect Genome-Phenome Analysis Platform (https://platform.rd-connect.eu/genomics/#/genomics). Likely pathogenic variants were identified applying standard filtering criteria: minor allele frequency less than 1% and high to moderate variant effect predictor. Shortlisted variants were interrogated for their predicted deleteriousness *in silico* and previous known association with human disease.

### Proteomic profiling

To elucidate cellular pathophysiological processes upon loss of functional WASHC4, proteomic profiling on human skin fibroblasts was performed utilizing a data-independent acquisition (DIA) approach as described previously [15], whereby control and *WASHC4*-patient fibroblast samples were processed and analyzed in parallel. For Gene Ontology (GO) term analysis, only those proteins identified as >2 or <0.5 fold-change with a significant *P* value were included.

### Coherent anti-Stokes Raman scattering microscopy and immunofluorescence

Ten-micrometer-thick sections were cut from a cryopreserved muscle biopsy specimen. Sections were used for immunofluorescence studies (as described previously [16] utilizing the antibodies listed in supplementary material, Table S2), for coherent anti-Stokes Raman scattering (CARS), and for second harmonic generation (SHG) microscopy. For CARS and SHG measurements, samples were dried under a constant flow of nitrogen gas, but no further sample preparation was applied.

All spectroscopic measurements were performed on a modified Leica (Wetzlar, Germany) TCS SP8 CARS laser scanning microscope (as described previously [15]). The generated CARS signals were detected both in backward and in forward direction (E- and F-CARS, respectively); the simultaneous SHG signal was detected in backward direction. A 40× water immersion objective (IRAPO 40×/1.10 water) was used for CARS and SHG imaging. CARS spectra were acquired for a field of 291 × 291 µm (2048 × 2048 pixels) by tuning the pump laser from 804.0 to 826.4 nm with a step size of 0.7 nm, a pixel dwell time of approximately 10 µs, and averaging of two images.

Immunofluorescence (IF) measurements were performed on the same instrument using an argon laser at 488 nm for excitation. Images were acquired with a 25× water immersion objective (Fluotar VISIR 25×/0.95 water) and fluorescence was detected with a hybrid detector from 500 to 600 nm. Fluorescence images were acquired with an image size of 465 × 465 µm (1024 × 1024 pixels) in the *x* and *y* direction.

### Statistical evaluation of muscle fiber calibers

Leica software LAS X (Version 2.0) was used for manual determination of the muscle fibers from the CARS images. For cross-sectioned muscle samples, the length and width of fully imaged fibers were determined, and the caliber was averaged from the two values. For muscle fibers in longitudinal section, the width of the fibers was taken as the caliber. A total of 638 fibers were analyzed for the patient. As a reference, 1457 fibers were analyzed from five control samples.

### Extraction of spectra for the determined features

The spectral CARS measurements were manually screened for conspicuous features. These were grouped according to their appearance (see the Results section). The CARS spectra in each group were first normalized and then averaged. CARS spectra were extracted for the area of the features as well as for inconspicuous areas neighboring the features, which were taken as normal

reference. All spectra per area were normalized to 1 and subsequently averaged. A total of 290 spectra were used for the spectra presented in the Results section: A: 59; B: 58; Ref: 38; Controls: 135.

### Data processing

The processing of the fluorescence measurements was performed using Matlab R2020a (MathWorks, Natick, MA, USA). For each image, the background was reduced by setting all data points showing less than 1% of intensity to this background threshold. Cosmic spikes were taken into account by defining an upper intensity threshold so that less than 0.1% of the data points above background intensity were above this upper threshold. Data points showing intensity above this value were set to the upper threshold. The entire image was then rescaled to the full range (8 bits).

Within each of the scaled images, 25 muscle fibers were selected using a manually defined irregular octagon. An intensity histogram analysis was performed for each of these muscle fibers. To account for the different sizes of the octagons, the histogram values were normalized to percentages. For each group, the mean and standard deviation were determined from the percentage values.

### Immunoblotting studies

Immunoblotting studies were performed as described previously [17] but utilizing nitrocellulose membrane. For each analysis, 10 µg of whole muscle protein extract was used. The primary antibodies and respective dilutions used are listed in supplementary material, Table S2. The secondary antibodies used were Alexa Fluor® 488 goat anti-rabbit (Abcam, Cambridge, UK), Invitrogen A-11034 (Thermo Fisher Scientific, Waltham, MA, USA); goat anti-mouse HRP (Thermo Fisher Scientific), Thermo G21040 (Thermo Fisher Scientific); and goat anti-rabbit HRP (Thermo Fisher Scientific), Thermo G21234 (Thermo Fisher Scientific).

## Results

### Clinical report

#### Family history

The parents are healthy, consanguineous (cousins I°), of Middle Eastern descent (United Arab Emirates). Neuromuscular, syndromic, or metabolic disorders in family history were denied. Their first child was a prematurely born (29 weeks of gestation) female, who died at 4 days of age due to unknown cause. They have two further daughters (Figure 1A), who are described thoroughly in the following sections and are listed in supplementary material, Table S1 as sibling 1 and sibling 2 (in total patients 11 and 12).

#### Sibling 1/WASHC4 patient 11

*Pregnancy and perinatal period*

The pregnancy was complicated because of hyperemesis gravidarum and intrauterine growth retardation. Birth was at 36 weeks of gestation due to poor results from cardiotocography (CTG). Birth weight was 1650 g ($-2.41z$), length was 46 cm ($-0.85z$), and head circumference was 31 cm ($-1.46z$) ($z$-scores [18]). Postnatally, a mild pulmonary adaption disorder (Apgar score and umbilical cord pH unknown), a poor suck, and jaundice requiring phototherapy were found. At the age of 28 days, significant muscle hypotonia and a complete lack of head control were noticed.

*Childhood development and diagnostics*

General development was delayed (only sounding; no sitting and reduced head control at 14 months; standing with support at 20 months). Clinical examination at 14 months showed dysmorphic features (epicanthus, low-set ears, microphthalmia, and retrognathia). Persisting feeding difficulties required insertion of a percutaneous endoscopic gastrostomy tube (PEG). Basic diagnostic work-up [echocardiography, electrocardiogram (ECG), nerve conduction velocity, laboratory values including creatine kinase (CK)], chromosome analysis, and electroencephalography (EEG) at 10 months showed no pathological findings, but brain magnetic resonance imaging (MRI) revealed agenesis of the pituitary gland. Due to abnormal brainstem-evoked response audiometry (BERA), hearing aids were implemented at the age of 5 years but were not well tolerated. Molecular karyotyping (Affymetrix Genome-Wide SNP_6.0 Array) showed no relevant dosage aberrations but revealed five large homozygous areas, encompassing about 98 Mb, which is in line with the known parental consanguinity. A muscle biopsy was performed at the age of 4 years (Figure 2).

At age 4.5 years, the patient developed epilepsy with generalized tonic–clonic seizures and received oxcarbazepine (seizure-free on therapy). From this age on, she was able to walk with support. At the age of 9 years, she presented with a global developmental delay with suspicion of severe ID, stereotypic movements, and autoaggression in combination with absent speech. It was never possible to perform a standardized intelligence quotient (IQ) test due to the profound ID. Short stature [height 121 cm ($-2.62z$)] and microcephaly (head circumference 49 cm ($-2.95z$)] but normal weight [26 kg ($-1.15z$)] ($z$-scores [18]) were found. She showed significant dysmorphic features such as an enlarged and coarsened nasal tip with deviation to the left side, a small upper lip vermilion, small eyes with moderate ptosis and mild strabismus, high arched eyebrows with discreet synophrys, as well as low-set ears with enlarged ear lobes and a prominent forehead with low-set hairline and hirsutism (Figure 1B,C,F,G). Clinical examination revealed areflexia and prominent generalized muscle hypotonia leading to right convex scoliosis (Figure 1D,E,F); contractures of the elbows,

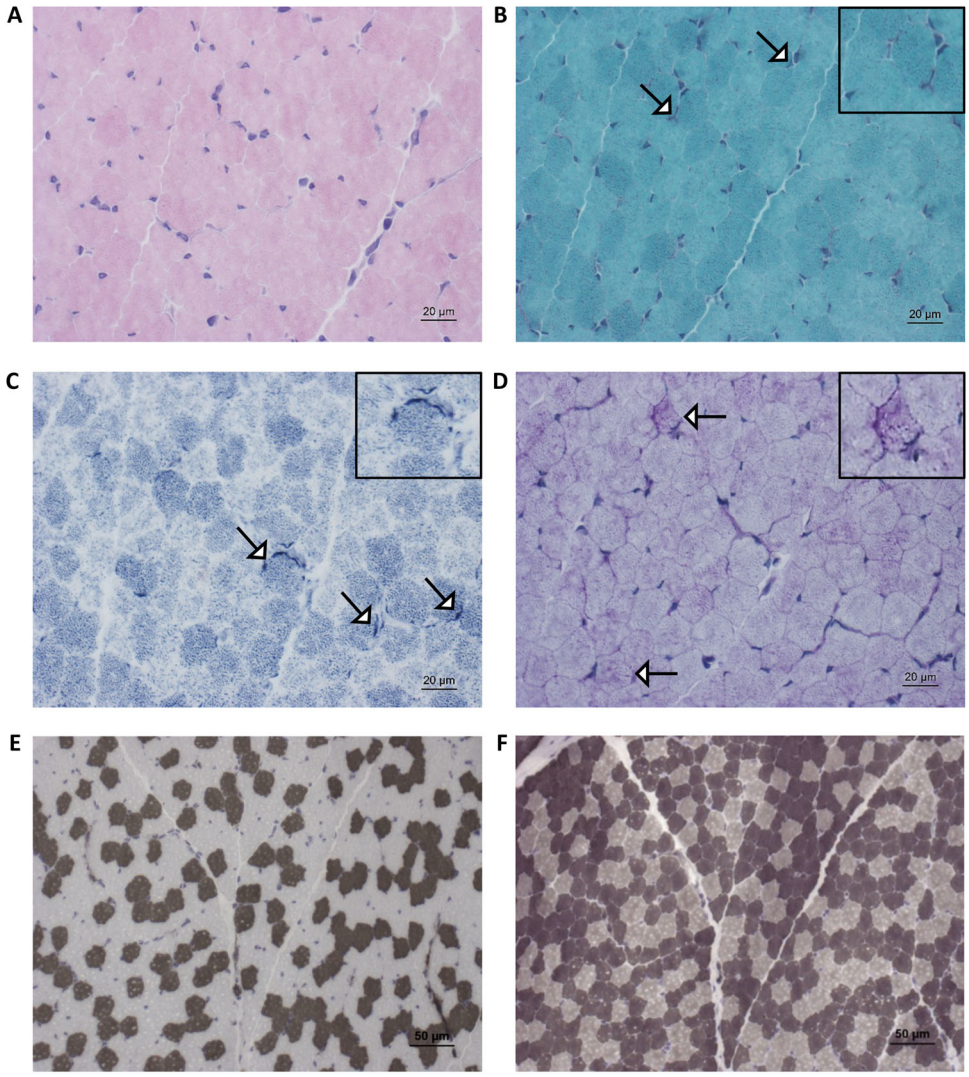


**Figure 2.** Muscle biopsy finding based on histological examination: (A) Hematoxylin and eosin (H&E) stain: musculature seen transversely and obliquely, preserved fascicle structure; perimysial connective tissue proliferation, no fat cell proliferation; no lymphohistiocytic cell infiltrates; muscle fibers polygonal, physiological fiber size variability, no fiber fragmentation or nuclear clumps; predominantly peripheral nuclei (centrally located nuclei <3%). No cell necrosis or basophil regenerating fibers; no ragged red fibers; no intracellular glycogen or lipid proliferation. (B) Modified Gomori stain shows occasionally the enrichment of mitochondria subsarcolemmally (white arrows). (C) Nicotinamide adenine dinucleotide hydrogen (NADH) stain shows increased subsarcolemmal reactivity in a minority of fibers (white arrows). (D) Periodic acid–Schiff (PAS) stain shows increased sarcoplasmic build-up on a minority of diseased muscle fibers (white arrows). (E, F) Adenosine triphosphatase (ATPase) stain (at pH 4.3 and 9.4) shows fiber-type disproportion (increased abundance of type 2 fibers). Insets show areas of interest in greater detail.

knees, and ankles; and she was only able to walk a few steps with support, with an unstable broad-based gait pattern.

*Pulmonary findings*

Due to frequent febrile pulmonary infections necessitating antibiotic treatment, additional diagnostic interventions (chest X-ray, polysomnography, anti-body investigations) were performed at the age of 4.5 years but did not identify an underlying cause. Computed tomography (CT) showed signs for a primary lung disease (thickened walls and ecstatic bronchi as well as milk glass opacity). During pulmonary infections, she presented with deterioration of motor skills and needed a long recovery time. In infection-free intervals, therapy was continued with antibiotic prophylaxis and anti-inflammatory therapy with azithromycin. Bronchoscopy showed signs of tracheomalacia. At the last appointment, the patient was 10 years of age and the parents reported only two upper airway infections during the last 6 months.

### Sibling 2/*WASHC4* patient 12

*Pregnancy and perinatal period*

The pregnancy was complicated with hyperemesis gravidarum and intrauterine growth retardation. Birth was at 37 weeks of gestation due to her sonographically estimated low body weight. Birth weight was 1800 g ($-2.78z$), length 46 cm ($-1.52z$), and head

circumference 31 cm ($-2.14z$) ($z$-scores [18]). She adapted well postnatally (Apgar 7 at 5 min and 9 at 10 min; umbilical cord pH 7.36), but developed feeding difficulties requiring the insertion of a nasogastric tube.

*Childhood development and diagnostics*

At age 8 months, she was only able to turn herself on her left side. Basic diagnostic work-up (laboratory parameters including CK, chromosome analysis, newborn screening, sonography of brain and abdomen, EEG) was without pathological findings. At the age of 12 months, she was equipped with hearing aids due to pathological BERA results. Due to persisting feeding difficulties and dystrophy ($-3.94z$), a PEG tube was inserted at the age of 22 months. Despite regular feeding via the PEG tube, she did not gain weight adequately. At 3.5 years, she presented with a severe global developmental delay with absent speech and dysmorphic stigmata (enlarged and coarsened nasal tip). At the age of 6 years, the patient was able to make her first unaided steps. At the age of 7 years, she presented with short stature (height 104 cm, $-3.79z$), dystrophy (weight 17 kg, $-2.56z$), and microcephaly (head circumference 49 cm, $-2.20z$) ($z$-scores [18]). She showed clearly visible dysmorphic features such as an enlarged and coarsened nasal tip with deviation to the right side, small eyes with moderate ptosis and low-set ears (Figure 1H,I), a global developmental delay with suspicion of severe intellectual disability (ID), and stereotypic movements in combination with absent speech. It was never possible to perform a standardized intelligence quotient (IQ) test due to the profound ID. Generalized hypotonia and areflexia were present. She was able to walk a few steps independently. At the age of 6 years, X-ray of her left hand showed a significantly retarded bone age, due to a low (not measurable) anti-Müllerian hormone (AMH) level; ovarian insufficiency was suspected and further controls were recommended. A cranial MRI was not performed until now.

*Pulmonary findings*

From the age of 21 months, she developed recurrent pulmonary infections, requiring frequent antibiotic therapy. Her sister had benefited from an anti-inflammatory treatment with oral azithromycin, which she also received. At the age of 6 years, it was stopped, due to unsatisfactory therapeutic success. Over the next years, recurrent pulmonary infections remained an ongoing problem, but in general the further course was stable.

### Comparison of WASHC4 patients and published cohorts

A comparison of the clinical symptoms of the two *WASHC4* patients described in this article with the patients previously described in the literature was performed to define commonalities and differences of their clinical features. This comparison is presented in supplementary material, Table S1 and revealed in total 43 different features. All patients (12 out of 12) had an abnormal speech development and ID. Short stature was present in 10 out of 12 patients. Patients 8–12 had a developmental delay and severely affected speech development in combination with borderline (patient 8), mild (patients 9 and 10), and severe ID (patients 11 and 12). Behavioral abnormalities were not mentioned by Ropers *et al* [10] but were described in four out of the remaining five patients. Moreover, the authors did not mention a developmental delay (including age of walking), deviating head circumference or dysmorphic features, whereas all patients described thereafter had clear dysmorphic features, for example a prominent and wide nasal tip (patients 8, 11, and 12), a prominent forehead and synophrys (patients 8, 9, and 10) or dysmorphic ears (patients 8 and 10). Hirsutism was present in patient 10 and patient 11 (but not in her sister, patient 12). Abnormalities of the bony hand skeleton were only present in the three patients described by Assoum *et al* [11]. Although dystrophy due to feeding difficulties was prominent in patients 11 and 12, this was not described by the other authors. While patient 8 developed macrocephaly, patients 10 and 11 showed microcephaly. Age of walking was slightly delayed in patients 8, 9, and 10 but was severely retarded in patients 11 and 12, with patient 11 still not being able to walk unassisted at the age of 9 years. Symptoms of a neuromuscular disease, as present in patient 11 (profound muscle hypotonia with suspicion of moderate muscle weakness, progressive scoliosis, multiple contractures), have not been reported in the literature thus far. As additional features, bilateral sensorineural hearing loss was present in patients 9, 11, and 12. Epilepsy was only mentioned in patient 11. Recurrent febrile pulmonary infections and endocrinological pathologies were only described in patients 11 and 12. Cranial MRI was performed in only 4 out of the 12 patients, and echocardiography in only 3 out of 12.

### Exome sequencing

WES data for the two affected sisters and their parents were analyzed, taking into account the family's consanguinity. Thus, filters were applied to select only rare (<1%) and damaging variants present in homozygosity in both siblings. Applying a medically interpretable gene panel ($n = 5419$), two missense candidate variants were identified: c.3041A>G; p.(Tyr1014Cys) in the *KIAA1033*/*WASHC4* gene and c.2396A>C; p.(Phe799Ser) in the *POSTN* gene, associated with myocardial infarction. The *WASHC4* variant is predicted to be deleterious by three *in silico* tools (SIFT, Polyphen2, and MutationTaster) and has a CADD score of 29, whereas the *POSTN* variant has a lower CADD score of 23.4, is predicted to be deleterious by two of the three tools tested, and has been reported as benign in ClinVar. All this makes the *WASHC4* missense change the only relevant candidate as disease-causing.

*Muscle histology*

Analysis of the quadriceps muscle biopsy revealed no significant changes by H&E staining (Figure 2A). Modified Gomori staining revealed subsarcolemmal accumulation of mitochondria in a minority of muscle fibers

(white arrows in Figure 2B). NADH staining revealed focal subsarcolemmal reactivity in some muscle fibers indicative of enrichment of mitochondria (Figure 2C). Periodic acid–Schiff reaction revealed increased sarcoplasmic reactivity in a minority of muscle fibers (white arrows in Figure 2D). The main finding is visible in the ATPase reaction (ATPase 4.3 and 9.4), which shows a fiber-type disproportion (increased abundance of type 2 fibers) (Figure 2E,F). Immunofluorescence-based analysis of several skeletal muscle proteins [caveolin-3; dystrophin 1, 2, and 3; alpha- and beta-dystroglycan; alpha-, beta-, gamma-, and delta-sarcoglycan; laminin-α2 (300 kDa and C-terminus); emerin; dysferlin; collagen VI (3C4 and VI-26); collagen IV; laminin-α5; utrophin; and neonatal myosin] showed no pathological findings (data not shown) and biochemical analysis of respiratory chain enzymes (complex I–IV) also did not show significant perturbations (data not shown).

### Global proteomic profiling of WASHC4 patient-derived fibroblasts

After demonstration of the expression of a variety of proteins of neuromuscular significance in human skin fibroblasts in one of our previous studies [15], we aimed to systematically address the suitability of these cells to study the molecular genesis of WASHC4-related pathology. Our approach allowed the quantification of 3707 proteins, out of which 364 (9.82%) were significantly dysregulated (Figure 3A,B). A total of 174 (4.69%) were significantly increased and 191 (5.13%) were significantly decreased (Figure 3B and supplementary material, Figure S1). The proteomic profiling data have been deposited at the ProteomeXchange Consortium via the PRIDE [19] partner repository with the dataset identifier PXD024222. To unravel underlying pathomechanisms, *in silico*-based pathway analyses were performed including gene ontology (GO) term analysis considering the increased and decreased proteins separately (Figure 3C).

### Cellular processes influenced by proteins with increased abundance

Our GO term-based analysis focusing on biological processes and cellular compartments revealed that proteins increased in the patient-derived cells are among others affecting extracellular matrix (ECM) organization and cell adhesion, protein folding and IRE1-mediated unfolded protein response, regulation of beta-amyloid clearance, positive regulation of (smooth) muscle cell proliferation, response to oxidative stress, and lipoprotein catabolic processes (Figure 3C, I + III). Moreover, an effect on the ECM and the cell membrane, the endoplasmic reticulum, endocytic vesicles, and mitochondria can be deduced from our *in silico* studies of increased proteins (Figure 3C, I + III). This molecular observation accords with the described role of the WASHC4 protein in the proper function of the endoplasmic/sarcoplasmic reticulum [20].

Focusing on proteins of neurological/neuromuscular relevance, it is important to note that a variety of such proteins that cause or are involved in the manifestation of neurological/neuromuscular disorders are increased in abundance. Among others, these proteins include apolipoprotein E [21], the SIL1-BiP chaperone complex [17], collagen alpha-1(VI) chain (MIM: 158810), neuropathy target esterase (MIM: 612020, 215470, and 245800), and sorting nexin-18, which stimulates the GTPase activity of DNM2 (MIM: 160150 and 606482) and promotes its location at the plasma membrane as well as tenascin [22] (supplementary material, Table S3). Interestingly, mutations in tenascin have been linked to sensorineural hearing loss [23], a clinical finding in our patients.

Of note, seven of the increased proteins belong to the ubiquitin system: ubiquitin-like protein ISG15, ubiquitin carboxyl-terminal hydrolase isozyme L1, E3 ubiquitin-protein ligase TRIM22, probable E3 ubiquitin-protein ligase makorin-2, small ubiquitin-related modifier 1, E3 ubiquitin-protein ligase TRIM56, and E3 ubiquitin-protein ligase UBR5 (supplementary material, Table S3).

### Cellular processes influenced by proteins with decreased abundance

*In silico* studies of proteins presenting with decreased abundance on GO term-based analysis focusing on biological processes and cellular compartments revealed that proteins that were decreased in the patient-derived cells are involved in cholesterol biosynthetic processes, mitochondrial function, actin filament bundle assembly, protein transport and vesicle-mediated transport with regulation of endocytosis, protein to membrane docking/membrane organization, as well as lysosome organization and autophagy (Figure 3C, II + IV). Moreover, an affliction of the cytoskeleton (actin filaments), mitochondria, sarcolemma, endosomes, endoplasmic reticulum, and particularly the lysosome (Figure 3C, II + IV) can be deduced. In addition, this molecular observation is in keeping with the described role of the WASHC4 protein in the proper function of the endoplasmic/sarcoplasmic reticulum [20] which might affect protein processing and clearance.

Focusing on proteins of neurological/neuromuscular relevance, it is worth noting that a variety of such proteins that cause or are involved in the manifestation of neurological/neuromuscular disorders are decreased in the patient-derived fibroblasts. Among others, these proteins include vacuolar protein sorting-associated protein 37A (MIM: 614898); plastin-3, a modifier of spinal muscular atrophy [24]; Ras-related protein Rab-7a (MIM: 600882); profilin-1 (MIM: 614808); lysosome-associated membrane glycoprotein 2 (MIM: 300257); delta-sarcoglycan (MIM: 601287); glycogen debranching enzyme (MIM: 232400); epsilon-sarcoglycan (MIM: 159900); persulfide dioxygenase ETHE1 (MIM: 602473); Golgi SNAP receptor complex member 2 (MIM: 614018); and lysosomal alpha-glucosidase (MIM: 232300).

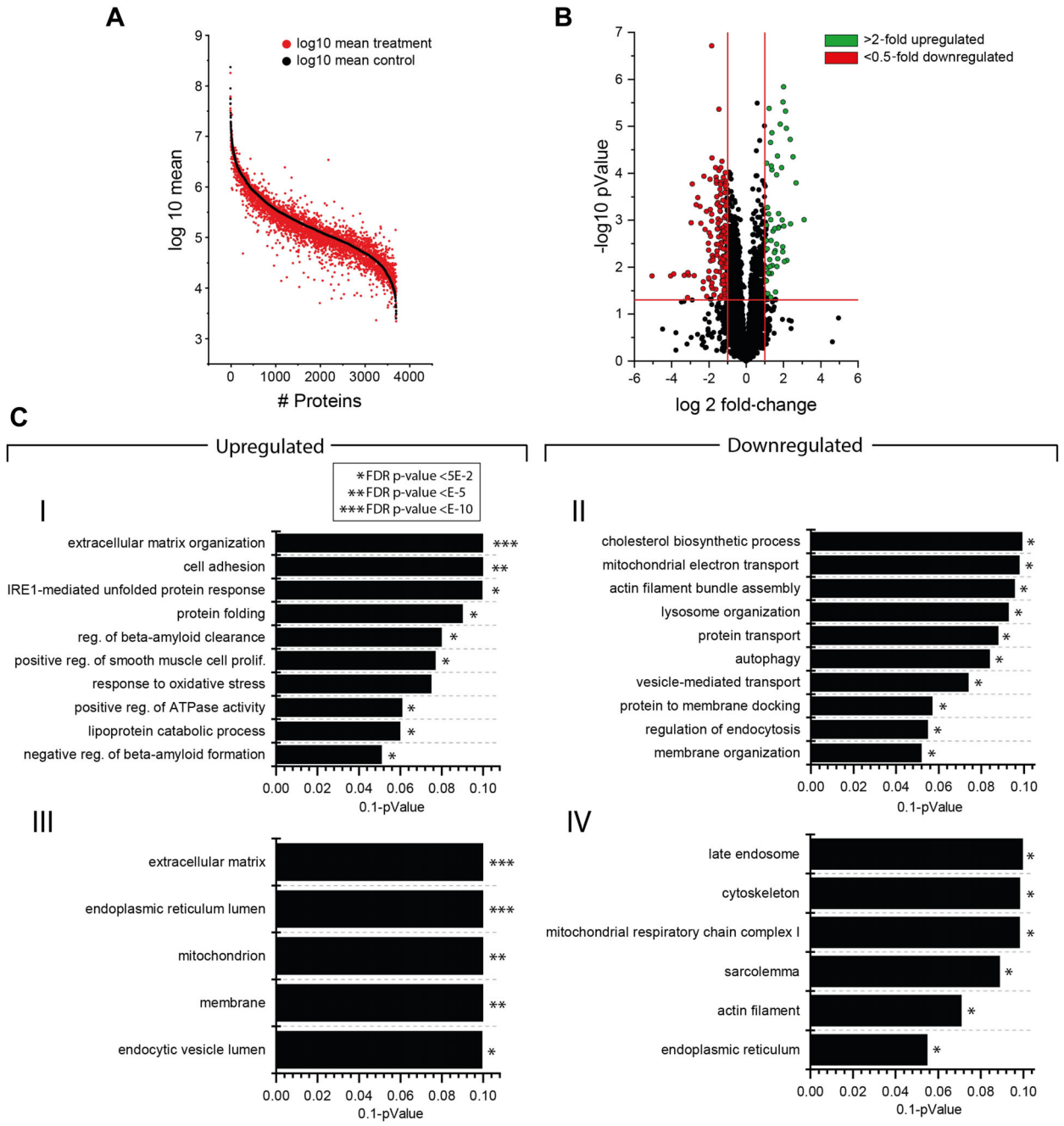


**Figure 3.** Proteomic profiling of WASHC4 patient-derived fibroblasts. (A) Protein enrichment plot along the entire abundance range. Proteins highlighted in black represent the results of control samples, sorted by abundance. Proteins highlighted in red represent the abundance of WASHC4 patient-derived fibroblasts, left in the same order as the proteins of the control samples to highlight differences in their expression. (B) Volcano plot of proteomic data depicting the $\log_2$ fold-change of identified proteins against the $-\log_{10}$ pValue. Red dots represent proteins showing a significant decrease, whereas green dots represent proteins with a significant increase in abundance by comparing control against WASHC4 patient-derived fibroblasts. (C) GO term analysis depicting different biological processes and cellular compartments significantly regulated by comparing control samples against WASHC4 patient-derived fibroblasts. Upregulated (I) and downregulated (II) biological processes, sorted by level of significance and enrichment, respectively. III and IV depict upregulated and downregulated cellular compartments, respectively.

Of note, mutations in V-type proton ATPase subunit B, a protein decreased in WASHC4 patient-derived fibroblasts, were linked to rare dominant developmental disorder characterized by facial dysmorphism with a bulbous nose, thick floppy ears, and intellectual disability (MIM: 616455).

## Validation of proteomic findings on a WASHC4 patient-derived muscle biopsy

Our global proteomic profiling revealed the altered expression of a variety of proteins known to be causative for or involved in the molecular genesis of neurological

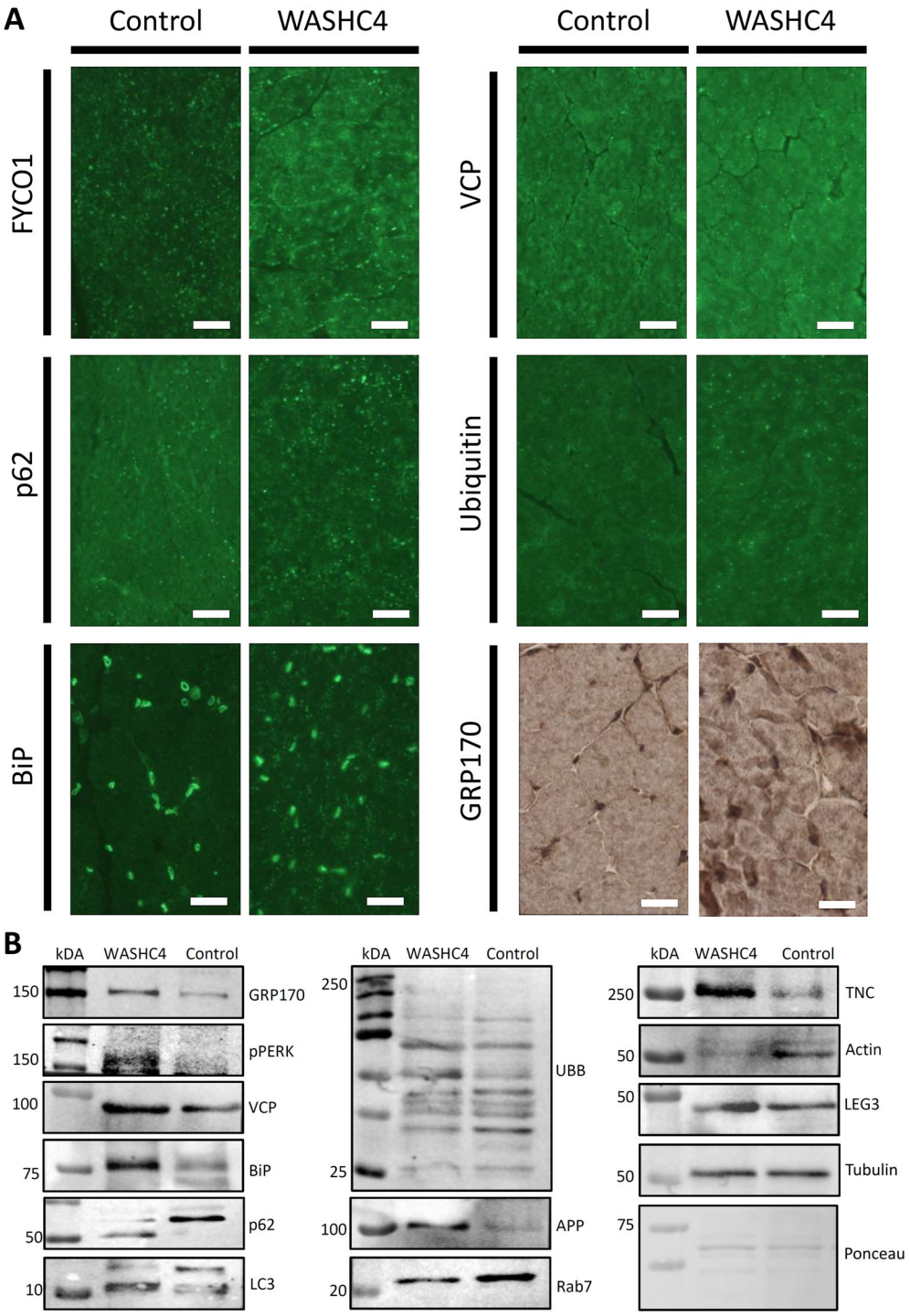


**Figure 4.** Immunological studies on WASHC4 patient-derived quadriceps muscle. (A) Immunostaining of FYCO1, p62, VCP, ubiquitin, BiP, and GRP170 reveals increased sarcoplasmic immunoreactivity in WASHC4-mutant muscle fibers. Scale bars = 30 μm. (B) Immunoblotting results confirming the increase of FYCO1, p62, VCP, ubiquitin, BiP, and GRP170 in whole protein extracts of the WASHC4 patient-derived muscle. LC3 showed an increased conversion from LC3-I to LC3-II in the WASHC4 patient-derived muscle. p62 showed a band at a lower molecular weight compared with the control. Additionally, there were increases of galectin-3 (LEG3), phospho-PERK (pPERK), and amyloid, as well as decreases of Rab7, actin, and tenascin (TNC). Ponceau staining of a representative nitrocellulose membrane demonstrates equal protein loading.

diseases. Therefore, an effect on proteins with known relevance for the development of neuromuscular diseases and/or known roles in modulation of the unfolded protein response and protein clearance was confirmed in a muscle biopsy derived from the same WASHC4-deficient patient exhibiting some myopathology already on the histological level [16]. Our immunofluorescence-based validation studies revealed sarcoplasmic increase of protein aggregation markers including FYCO1, VCP, p62, and ubiquitin as an important interactor of WASHC4 (Figure 4A). In addition, an increase of BiP, a major chaperone

modulating the ER stress response, confirmed the result of proteomic profiling in patient fibroblasts. In support of this finding, we detected an increase of its co-chaperone GRP170 in the quadriceps biopsy derived from the same patient. Immunoblotting confirmed the microscopic findings and, moreover, revealed an elevated conversion of LC3-I to LC3-II; an increase of the phosphorylated form of PERK (pPERK), indicative of the presence of perturbed (ER/SR) proteostasis; and an increase of amyloid, suggesting protein aggregate formation (Figure 4B).

Immunofluorescence-based quantitative histogram analysis for the WASHC4 patient and a healthy individual was performed. The analysis revealed for BiP staining that the patient muscle fibers show a higher percentage of high fluorescence signal intensities, indicative of an increase of this UPR-relevant protein in WASHC4-mutant muscle fibers (Figure 5A). For p62 staining, the WASHC4 patient showed slightly lower signal intensities but simultaneously a higher percentage of points with maximum signal intensity along with sarcoplasmic clustering, supporting the concept of protein aggregation (Figure 5B). Remarkably, immunoblotting showed p62 appearing with a band at a lower molecular weight in the muscle protein extract of the patient compared with the control (Figure 4B).

The ECM protein tenascin, implicated in the guidance of migrating neurons, synaptic plasticity, and neuronal regeneration, was also identified to be increased in WASHC4-deficient patient-derived fibroblasts and the sarcoplasmic increase could be confirmed in quadriceps muscle fibers derived from the same patient (Figure 4B and supplementary material, Figure S1). Prompted by our proteomic findings suggesting a decrease of the actin cytoskeleton, phalloidin staining (visualizing the actin cytoskeleton) was performed in the WASHC4 patient-derived quadriceps biopsy, which revealed less intensive immunoreactivity suggesting a decrease of actin cytoskeleton in WASHC4-diseased muscle fibers (supplementary material, Figure S1). Actin decrease was also confirmed by immunoblotting (Figure 4B). Galectin-3 coordinates the mobilization of core autophagy regulators in response to damaged endomembranes and was identified as decreased in WASHC4 patient-derived fibroblasts; confirmational immunological studies on the patient-derived quadriceps biopsy confirmed a decrease of galectin-3 (Figure 4B and supplementary material, Figure S1). Along this line, two further proteins involved in autophagy, RAB7 and CD63, were decreased in WASHC4 patient-derived fibroblasts and a similar decrease was confirmed in the patient-derived muscle biopsy (Figure 4B and supplementary material, Figure S1). Proteomic profiling revealed an increase of collagen VI in fibroblasts and confirmational studies on the patient-derived quadriceps biopsy showed an increase of collagen VI within the ECM (supplementary

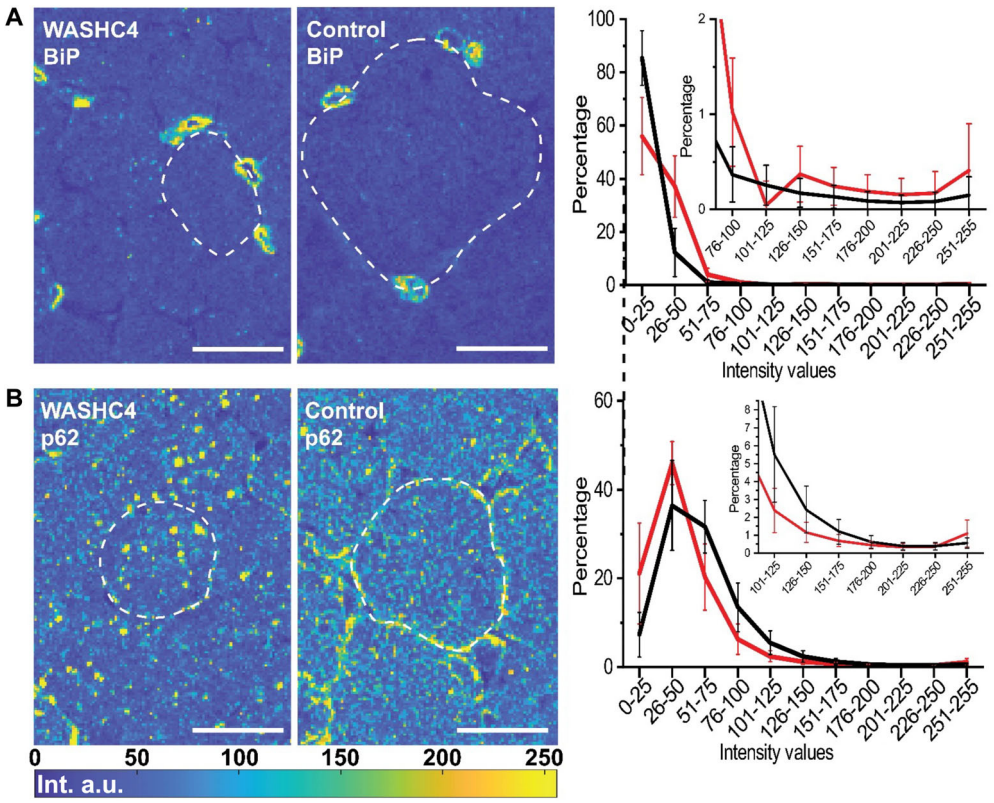


Figure 5. Single muscle fiber histogram analysis: (A) BiP and (B) p62. Representative rescaled fluorescence images (see Materials and methods) of muscle from the patient (left) and a healthy individual (center). Representative fibers are framed with dashed lines for better visualization. Right: intensity histogram of the processed fluorescence images. The mean value and standard deviation from 25 single cells per sample are shown for the patient (red) and the control (black) sample. Scale bars: 25 µm.

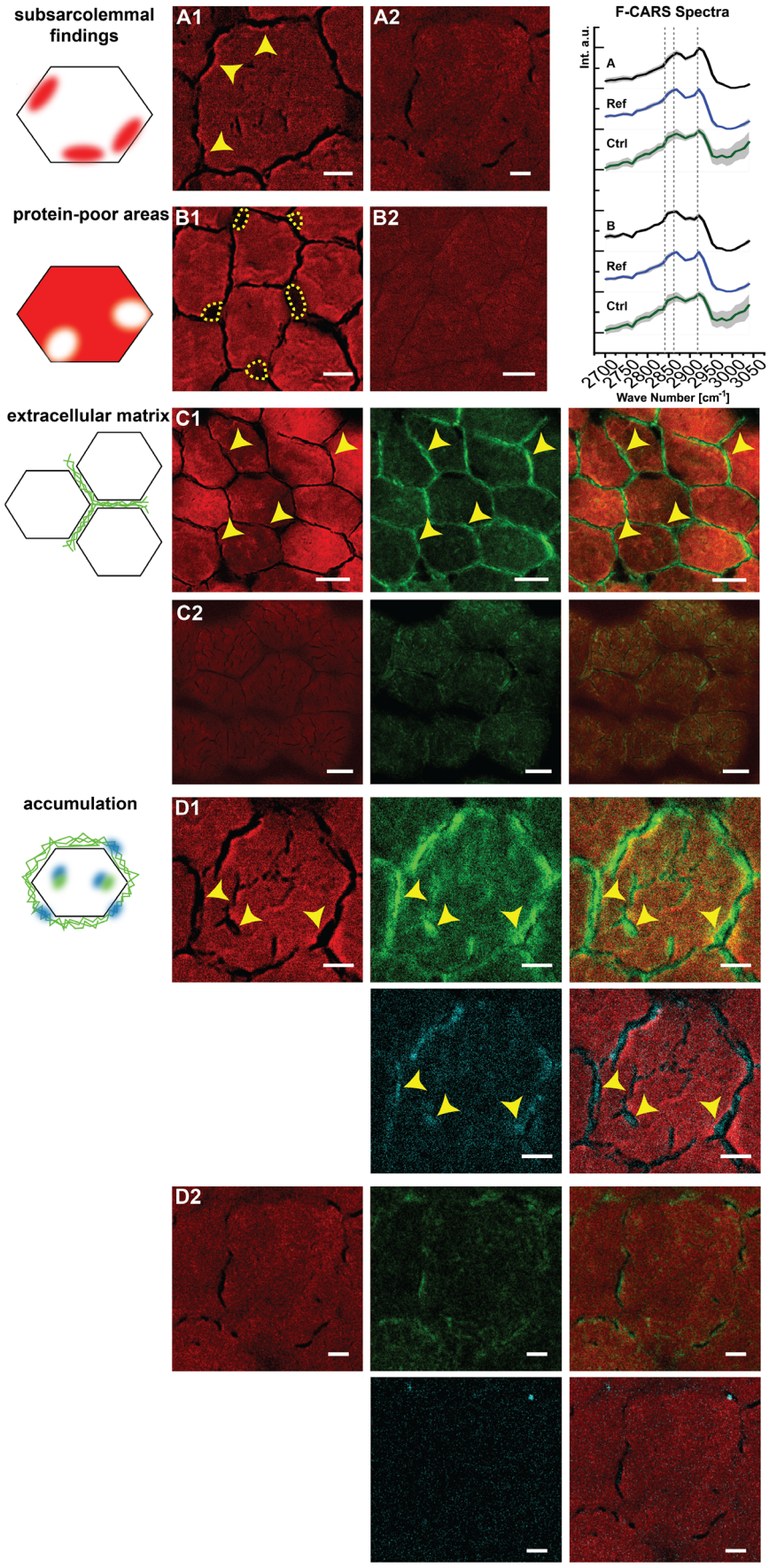


Figure 6 Legend on next page.

material, Figure S1). This molecular observation may reflect fibrosis, which is compatible with the muscle involvement upon loss of functional WASHC4. Also, results using CARS indicate the presence of mild fibrosis (see below).

### CARS microscopy on WASHC4 patient-derived muscle biopsy

Coherent anti-Stokes Raman scattering is a nonlinear variant of the Raman effect. It allows the targeted analysis of molecule-specific vibrations and thus can yield information on the chemical composition of a sample. Second harmonic generation (SHG) is also a nonlinear spectroscopic method. An SHG signal indicates highly organized substances, for example, collagen [25] or ordered protein aggregates [26]. We applied a multimodal approach utilizing both nonlinear methods to analyze the morphology and biochemical composition of muscle biopsies non-destructively without any staining, labeling or pretreatment.

From the CARS measurements of the patient's muscle biopsy, an average muscle fiber caliber of $22.81 \pm 3.92$ µm (638 fibers) was determined. From comparison with the average muscle fiber caliber of five healthy individuals ($43.92 \pm 23.29$ µm; 1457 fibers), the patient displays atrophic muscle fibers.

Within the patient biopsy, we detected a total of four spectroscopically distinct features (Figure 6). In 581 of 638 (91%) fibers from the patient, we observed subsarcolemmal regions of increased signal intensity of the symmetric $=CH_3$ vibration at 2921 $cm^{-1}$ compared with the signals at 2868 and 2847 $cm^{-1}$ (Figure 6A1).

Given that this signal is characteristic for proteins [27,28], this microscopic finding indicates an increased protein content at these positions, thus pointing towards protein aggregation. The signals at 2868 and 2847 $cm^{-1}$ result from $=CH_2$ vibrations and are mainly associated with lipids [29,30]. Only 55 of 1457 fibers (3.77%) in the control samples showed a comparable finding.

We point out that protein aggregation is only detectable when the signal from the respective structures is larger than the signal from the fiber background. In addition to protein aggregates, other $=CH_3$ substances exist in cells from which signals are detected. In addition, the differentiation between certain proteins using CARS has not been followed here. Thus, aggregations of certain proteins, e.g. FYCO1, p62, or BiP, may be visible by fluorescence staining but do not alter the total protein concentration enough to be visible in the CARS image.

We also found areas of decreased signal intensity at 2921 $cm^{-1}$ in the subsarcolemmal region in the patient (Figure 6B1). These areas tend to have a roundish shape. Since only the CARS signal intensity at 2921 $cm^{-1}$ is decreased but not the intensity of the signal at 2868 $cm^{-1}$, we assume these areas to be protein-poor lumens surrounded by membranes. We were able to characterize these regions as enlarged nuclei by subsequent H&E staining of the same sample (Figure 2A). Between all muscle fibers of the patient, we detected a strong SHG signal (Figure 6C1) indicating the presence of collagen. Since collagen is a component of the ECM, this points toward an increase in the ECM in the area around the muscle fibers. Lastly, in some regions, a CARS signal at 2921 $cm^{-1}$ was detected in backward direction (E-CARS) with no corresponding signal intensity in F-CARS (Figure 6D1, cyan), but co-localizing with the SHG signal (Figure 6D1, green). Since it is known that E-CARS allows the imaging of small objects, which are not detected in F-CARS [31], these positions may indicate areas with very small objects present and may potentially represent the accumulation of proteins. These regions are found within the fibers as well as in the ECM.

## Discussion

A clinical comparison of the two *WASHC4* patients described here with those previously reported in the literature was performed. This revealed that the most frequent common symptoms include poor language skills/language delay (12/12) and ID (12/12), followed by short stature (10/12). Ropers *et al* did not report developmental delay, deviating head circumference, behavioral abnormalities, or dysmorphic features [10], whereas all patients described thereafter showed these symptoms, including clear dysmorphic features. The two patients

**Figure 6.** Spectroscopic findings in the muscle biopsies of the WASHC4 patient determined from CARS and SHG. (A1) Subsarcolemmal regions of patient fiber with increased CARS signal in the forward direction (F-CARS) at 2921 $cm^{-1}$ (marked with arrowheads; scale bar: 6 µm). (A2) Fiber of a control without subsarcommal regions with increased CARS signal (scale bar: 5 µm). (B1) Subsarcolemmal areas of patient fibers with low F-CARS signal intensity at 2921 $cm^{-1}$. The roundish areas are surrounded by dotted lines (scale bar: 8 µm). (B2) Fibers of a control without roundish areas with low F-CARS signal at 2931 $cm^{-1}$ (scale bar: 20 µm). For A1 and B1, respectively, a spectrum derived from the areas with altered F-CARS signal is shown on the far right. A corresponding reference spectrum (Ref) was derived from an area of the patient's muscle fiber that showed no abnormalities. In addition, a spectrum of the controls (Ctrl) is shown. Spectra were normalized and then averaged. The standard deviation is shown in grey. The vertical dotted lines highlight the wavenumbers 2847, 2868, and 2921 $cm^{-1}$. (C1, C2) F-CARS (red), SHG (green), and both merged channels. (C1) Strong SHG signals are observed between the muscle fibers of the patient (marked with arrowheads; scale bars: 15 µm). (C2) Control without strong SHG signal between fibers (scale bars: 15 µm). (D1, D2) F-CARS (red), SHG (green), CARS image detected in the backward direction (E-CARS, cyan), and combinations of merged channels. (D1) Strong signals are present in the ECM as well as in the muscle fibers of the patient. The signals of SHG and E-CARS are partially co-localized (indicated by arrowheads; scale bars: 5 µm). (D2) Corresponding images of the three channels of a control for comparison with D1 (scale bars: 5 µm). The displayed images are averages from three acquisitions and were taken at 811 nm corresponding to 2932 $cm^{-1}$ for CARS measurements, representing protein distribution.

described in this study showed a very significant motor delay and failure to develop speech in combination with a profound ID (not possible to be tested with a standardized test).

Based on the report of further patients and our study, in total 27 different features were described. The majority of these features were present in only some of the patients – some features even only in single patients. Along this line, the clinical report of the patients presented in this study expands the phenotypical spectrum of *WASHC4* patients by adding ptosis (as seen in patients with neuromuscular junction defects), muscle weakness, scoliosis, and contractures in combination with fiber-type disproportion (as seen, for example, in congenital myopathies) and protein dysregulation as well as recurrent pulmonary infections, epilepsy, and various endocrinological features to the list of clinical features. Our data confirm the broad clinical spectrum of *WASHC4* variants and highlight the need for accurate clinical phenotyping to improve understanding of the burden and pathological mechanisms of genetic diseases.

In keeping with the phenotype, one might speculate that protein folding and dysregulation impact the manifestation of different symptoms associated with this disorder. To identify proteins, which are affected by loss of functional WASHC4, proteomic profiling was carried out on skin fibroblasts derived from a *WASHC4* patient. This approach was prompted by the molecular observation that a variety of proteins of neurological relevance are expressed in these cells [15]. Indeed, our proteomic study indicated altered expression of numerous proteins decisive for proper function of the neuromuscular axis (supplementary material, Table S3). This molecular finding not only provides first insights into the biochemical origin of the broad neurological involvement of WASHC4 deficiency but also confirms the suitability of fibroblasts for identifying pathophysiological processes of neuronal relevance [15]. Along this line, these data suggest that a molecular interplay of dysregulated proteins might contribute to the clinical manifestation of symptoms. So far, muscle fiber involvement upon loss of functional WASHC4 has 'only' been indicated by *in vivo* studies utilizing a zebrafish model [9]. Remarkably, confirmational studies of our proteomic findings obtained in human skin fibroblasts on a quadriceps biopsy of the same patient confirmed dysregulations of paradigmatic proteins analyzed, indicating impaired ER function/presence of ER stress and build-up of protein aggregation markers along with a decrease of autophagy modulators. Decreased phalloidin staining in muscle strongly supports the relevance of decreased cytoskeleton proteins detected in fibroblasts. The presence of small protein aggregates was also detected by CARS microscopy. Moreover, an affliction of the skeletal muscles is indicated by our histological findings showing a reduction in succinate dehydrogenase (SDH) and an increase of type 2 fibers as well as by the calculation of muscle fiber diameter indicating atrophy. Taken together, these findings highlight that skeletal muscles also are affected – defined by profound protein dysregulations and impaired protein processing and clearance. Given that modulation of ER function and protein clearance became promising targets in preclinical and clinical studies applying, for instance, chemical chaperones [32], our findings suggest that this approach might also represent a starting point in the testing of interventional concepts for WASHC4-associated disease. The patient-derived fibroblasts might serve as a valuable *in vitro* model for pre-clinical studies. Protein dysregulations might also explain non-neurological manifestations: mutations in V-type proton ATPase subunit B were linked to intellectual disability complicated by facial dysmorphisms with a bulbous nose and thick floppy ears (MIM: 616455), clinical findings which are also present in our patients.

However, the investigation of additional fibroblast cultures and muscle biopsies derived from WASHC4 patients (or animal models) would be needed to define the above-mentioned pathological mechanisms as commonly associated with loss of functional WASHC4 in different cellular populations. Further proteomic studies on different cellular populations and tissues would allow us to identify pathophysiological cascades (and rescue mechanisms) which are shared or are specific.

## Acknowledgements

We are grateful to the family for their cooperation and for their permission to publish the data and photographs. Four authors of this publication are members of the European Reference Network for Neuromuscular Diseases – Project ID No 870177. We thank Mr Tobias Schroeder, Mr Fabian Förster, Mrs Swantje Hertel, and Mrs Regina Kubica for expert technical assistance. This study was supported by the 'Ministerium für Kultur und Wissenschaft des Landes Nordrhein-Westfalen', the 'Regierenden Bürgermeister von Berlin – Senatskanzlei Wissenschaft und Forschung', and the 'Bundesministerium für Bildung und Forschung', also in form of the Leibniz Research Cluster (grant number 031A360E). This work was also supported by a grant from the French Muscular Dystrophy Association (AFM-Téléthon) (#21466) to AR. RH was supported by the European Research Council (309548), a Wellcome Investigator Award (109915/Z/15/Z), the Medical Research Council (UK) (MR/N025431/1), the Wellcome Trust Pathfinder Scheme (201064/Z/16/Z), the Newton Fund (UK/Turkey, MR/N027302/1), the Lily Foundation, and the Evelyn Trust. HL receives support from the Canadian Institutes of Health Research (Foundation Grant FDN-167281), the Canadian Institutes of Health Research and Muscular Dystrophy Canada (Network Catalyst Grant for NMD4C), the Canada Foundation for Innovation (CFI-JELF 38412), and the Canada Research Chairs program (Canada Research Chair in Neuromuscular Genomics and Health, 950-232279). Parts of this study were financed within the framework of the NME-GPS project by the European Regional

Development Fund (ERDF). AT is supported by the Horizon 2020 research and innovation program via grant 779257 'Solve-RD'. Sequencing and analysis were provided by the Broad Institute of MIT and Harvard Center for Mendelian Genomics (Broad CMG) and were funded by the National Human Genome Research Institute, the National Eye Institute, and the National Heart, Lung and Blood Institute grant UM1 HG008900, and in part by National Human Genome Research Institute grant R01 HG009141.

## Author contributions statement

AG and AR conceptualized and designed the study, drafted the first version of the manuscript, interpreted results and were principally responsible for the final content. HK, USS, AS, FS, CK and AK revised the manuscript for important intellectual content. AT, AO, HL, JC, UM, AC and AH conducted assays, analyzed data and interpreted results. All the authors were involved in writing the paper and had final approval of the submitted and published versions.

## Data availability statement

Proteomic data have been uploaded to ProteomeXchange via the PRIDE Archive and are accessible using the dataset identifier PXD024222 (https://www.ebi.ac.uk/pride/archive/projects/PXD024222); molecular genetic data have been uploaded to RD-Connect (https://platform.rd-connect.eu/), reference number P0018471.

## References

1. Leonard H, Wen X. The epidemiology of mental retardation: challenges and opportunities in the new millennium. *Ment Retard Dev Disabil Res Rev* 2002; **8:** 117–134.
2. Clemen CS, Tangavelou K, Strucksberg KH, *et al*. Strumpellin is a novel valosin-containing protein binding partner linking hereditary spastic paraplegia to protein aggregation diseases. *Brain* 2010; **133:** 2920–2941.
3. Elliott AM, Simard LR, Coghlan G, *et al*. A novel mutation in *KIAA0196*: identification of a gene involved in Ritscher–Schinzel/3C syndrome in a First Nations cohort. *J Med Genet* 2013; **50:** 819–822.
4. Marchand JB, Kaiser DA, Pollard TD, *et al*. Interaction of WASP/Scar proteins with actin and vertebrate Arp2/3 complex. *Nat Cell Biol* 2001; **3:** 76–82.
5. Jia D, Gomez TS, Metlagel Z, *et al*. WASH and WAVE actin regulators of the Wiskott–Aldrich syndrome protein (WASP) family are controlled by analogous structurally related complexes. *Proc Natl Acad Sci U S A* 2010; **107:** 10442–10447.
6. Linardopoulou EV, Parghi SS, Friedman C, *et al*. Human subtelomeric WASH genes encode a new subclass of the WASP family. *PLoS Genet* 2007; **3:** e237.
7. Kelleher JF, Atkinson SJ, Pollard TD. Sequences, structural models, and cellular localization of the actin-related proteins Arp2 and Arp3 from Acanthamoeba. *J Cell Biol* 1995; **131:** 385–397.
8. Derivery E, Gautreau A. Evolutionary conservation of the WASH complex, an actin polymerization machine involved in endosomal fission. *Commun Integr Biol* 2010; **3:** 227–230.
9. Kustermann M, Manta L, Paone C, *et al*. Loss of the novel Vcp (valosin containing protein) interactor Washc4 interferes with autophagy-mediated proteostasis in striated muscle and leads to myopathy *in vivo*. *Autophagy* 2018; **14:** 1911–1927.
10. Ropers F, Derivery E, Hu H, *et al*. Identification of a novel candidate gene for non-syndromic autosomal recessive intellectual disability: the WASH complex member SWIP. *Hum Mol Genet* 2011; **20:** 2585–2590.
11. Assoum M, Bruel AL, Crenshaw ML, *et al*. Novel *KIAA1033/WASHC4* mutations in three patients with syndromic intellectual disability and a review of the literature. *Am J Med Genet A* 2020; **182:** 792–797.
12. Reuter MS, Tawamie H, Buchert R, *et al*. Diagnostic yield and novel candidate genes by exome sequencing in 152 consanguineous families with neurodevelopmental disorders. *JAMA Psychiatry* 2017; **74:** 293–299.
13. Kikuno R, Nagase T, Ishikawa K, *et al*. Prediction of the coding sequences of unidentified human genes. XIV. The complete sequences of 100 new cDNA clones from brain which code for large proteins *in vitro*. *DNA Res* 1999; **6:** 197–205.
14. Courtland JL, Bradshaw TW, Waitt G, *et al*. Genetic disruption of WASHC4 drives endo-lysosomal dysfunction and cognitive-movement impairments in mice and humans. *Elife* 2021; **10:** e61590.
15. Hentschel A, Czech A, Münchberg U, *et al*. Protein signature of human skin fibroblasts allows the study of the molecular etiology of rare neurological diseases. *Orphanet J Rare Dis* 2021; **16:** 73.
16. Roos A, Hathazi D, Schara U. Immunofluorescence-based analysis of caveolin-3 in the diagnostic management of neuromuscular diseases. *Methods Mol Biol* 2020; **2169:** 197–216.
17. Roos A, Buchkremer S, Kollipara L, *et al*. Myopathy in Marinesco–Sjögren syndrome links endoplasmic reticulum chaperone dysfunction to nuclear envelope pathology. *Acta Neuropathol* 2014; **127:** 761–777.
18. Kromeyer-Hauschild K, Wabitsch M, Kunze D, *et al*. Perzentile für den Body-mass-Index für das Kindes- und Jugendalter unter Heranziehung verschiedener deutscher Stichproben. *Monatsschr Kinderheilkd* 2001; **149:** 807–818.
19. Perez-Riverol Y, Csordas A, Bai J, *et al*. The PRIDE database and related tools and resources in 2019: improving support for quantification data. *Nucleic Acids Res* 2019; **47:** D442–D450.
20. Kind B, Koehler K, Lorenz M, *et al*. The nuclear pore complex protein ALADIN is anchored via NDC1 but not via POM121 and GP210 in the nuclear envelope. *Biochem Biophys Res Commun* 2009; **390:** 205–210.
21. Huynh TV, Davis AA, Ulrich JD, *et al*. Apolipoprotein E and Alzheimer's disease: the influence of apolipoprotein E on amyloid-β and other amyloidogenic proteins. *J Lipid Res* 2017; **58:** 824–836.
22. Aktar R, Peiris M, Fikree A, *et al*. The extracellular matrix glycoprotein tenascin-X regulates peripheral sensory and motor neurones. *J Physiol* 2018; **596:** 4237–4251.
23. Zhao Y, Zhao F, Zong L, *et al*. Exome sequencing and linkage analysis identified tenascin-C (TNC) as a novel causative gene in nonsyndromic hearing loss. *PLoS One* 2013; **8:** e69549.
24. Oprea GE, Kröber S, McWhorter ML, *et al*. Plastin 3 is a protective modifier of autosomal recessive spinal muscular atrophy. *Science* 2008; **320:** 524–527.
25. Ajeti V, Nadiarnykh O, Ponik SM, *et al*. Structural changes in mixed Col I/Col V collagen gels probed by SHG microscopy: implications for probing stromal alterations in human breast cancer. *Biomed Opt Express* 2011; **2:** 2307–2316.
26. Wampler RD, Kissick DJ, Dehen CJ, *et al*. Selective detection of protein crystals by second harmonic microscopy. *J Am Chem Soc* 2008; **130:** 14076–14077.

27. Cheng JX, Xie XS. Vibrational spectroscopic imaging of living systems: an emerging platform for biology and medicine. *Science* 2015; **350:** aaa8870.
28. González Coraspe JA, Weis J, Anderson ME, *et al*. Biochemical and pathological changes result from mutated caveolin-3 in muscle. *Skelet Muscle* 2018; **8:** 28.
29. Rinia HA, Burger KN, Bonn M, *et al*. Quantitative label-free imaging of lipid composition and packing of individual cellular lipid droplets using multiplex CARS microscopy. *Biophys J* 2008; **95:** 4908–4914.
30. Chughtai AA, Kaššák F, Kostrouchová M, *et al*. Perilipin-related protein regulates lipid metabolism in *C. elegans*. *PeerJ* 2015; **3:** e1213.
31. Cheng JX, Jia YK, Zheng G, *et al*. Laser-scanning coherent anti-Stokes Raman scattering microscopy and applications to cell biology. *Biophys J* 2002; **83:** 502–509.
32. Brandvold KR, Morimoto RI. The chemical biology of molecular chaperones – implications for modulation of proteostasis. *J Mol Biol* 2015; **427:** 2931–2947.

## SUPPLEMENTARY MATERIAL ONLINE

**Supplementary figure legend**

**Figure S1.** Immunostaining studies of WASHC4 patient-derived quadriceps muscle

**Table S1.** Clinical comparison of sibling 1 and sibling 2 (in total *WASHC4* patients 11 and 12) with the *WASHC4* patients previously described in the literature

**Table S2.** Primary antibodies used in this study

**Table S3.** List of proteins dysregulated in skin fibroblasts derived from one *WASHC4* patient